Applied Catalysis A, General 694 (2025) 120151

Contents lists available at ScienceDirect

Applied Catalysis A, General

journal homepage: www.elsevier.com/locate/apcata

Reusability of Mg/Al catalysts for the aldol condensation of furfural and acetone in a continuous flow reactor

Saleem Munir, Daniel Montané *, Magdalena Constantí, Francesc Medina

Departament d'Enginyeria Química, Universitat Rovira i Virgili, Avinguda dels Països Catalans 26, Tarragona E-43007, Spain

ARTICLE INFO

Keywords:
Biofuel production
Heterogeneous basic catalysis
Rehydrated hydrotalcite
Layered double hydroxide
Catalyst reactivation

ABSTRACT

Hydrotalcite catalysts with a Mg: Al ratio of 3:1 were assessed for the aldol condensation of furfural with acetone on a continuous packed bed reactor. The as-prepared (FHT), calcined (CHT), and rehydrated (RHT) hydrotalcites were characterized and their activity was tested at 100 °C and 12 bar(a) with an acetone:furfural ratio of 10:1 at a furfural WHSV of 5.77 h^{-1}. FHT showed low conversion and deactivated fast. CHT and RHT exhibited complete conversion during 2 and 4 h, respectively, and deactivated to a 20 % conversion after 8–11 h. The main products were (*E*)-4-(furan-2-yl)but-3-en-2-on (C8) and (1*E*,4*E*)-1,5-di(furan-2-yl)penta-1,4-dien-3-one (C13). Small amounts of higher molar mass products formed by ketonization were observed, and they were linked to the deposition of insoluble oligomers. Reuse of the spent catalysts by recalcination to remove the organic deposits was evaluated for a total of four reaction tests. A gradual loss of performance was seen after each reactivation treatment.

1. Introduction

The impact of anthropogenic emissions on climate change and the eventual depletion of fossil fuels have prompted the search for alternative sources to meet the demand of primary energy and materials [1,2]. Vegetable biomass is the sole natural source of organic carbon, and it is hence envisioned as the natural substitute to fossil resources to produce renewable chemicals and fuels. The transformation of biomass into basic building blocks for the chemical industry requires conversion routes different from those existing for fossil resources. Unlike oil and natural gas, biomass is formed by highly oxygenated polymers: cellulose and hemicellulose, which constitute the carbohydrate fraction of biomass, and lignin that is a random heteropolymer made by cross-linked phenolic precursors. Because of the chemical heterogenicity of the biomass constituents, a combination of several multistep processes is needed to fully convert biomass to useable products [3–5]. Furfural is the main chemical produced commercially from hemicellulose. It results from the hydrolysis and dehydration of the pentoses forming hemicellulose in some food crop residues and hardwoods. The main industrial application of furfural is as precursor to synthesize furfuryl alcohol, and it is also used as solvent and in the synthesis of other furans such as furan, methyl-furan, acetyl-furan and furoic acid [6,7]. Furfural is versatile for chemical transformations due to the reactivity conferred by the aldehyde group and the heteroaromatic furan ring, and it was identified as one of the top value-added chemicals obtained from a carbohydrate platform biorefinery [4]. Furfural can be converted to an extensive array of chemicals. The aromatic furan ring can be subjected to hydrogenation, ring-opening hydrogenolysis, oxidation, alkylation, halogenation, and nitration, while the aldehyde group facilitates its transformation by decarbonylation, aldol and Knoevenagel condensations, oxidation to carboxylic acids, and hydrogenation to alcohols. Detailed discussions of the state of the art and the latest advances in catalysis for the conversion of furfural through those routes have been presented in recent review articles, both for processes based on conventional catalysis [8–14] and based on biocatalysis with microorganisms and enzymes [13,14]. The use of furfural and hydroxymethyl furfural for the synthesis of drop-in fuels [15], and particularly sustainable aviation fuels (SAF) [7,16], is receiving significant attention. The production of alkanes in the jet-fuel range (C7-C18) from furfural can be performed through carbon-carbon coupling reactions like hydroxyalkylation/alkylation and aldol condensation, followed by hydrogenation of the resulting oxygenated adducts [17,18]. Acetone is suited for aldol condensation with furfural since it yields C8 and C13 molecules [3,19,21–25], and it can be obtained from biomass as well through fermentation or by catalytic conversion of bio-based feedstocks [20].

The aldol condensation between furfural and acetone involves the

* Corresponding author.
E-mail address: daniel.montane@urv.cat (D. Montané).

https://doi.org/10.1016/j.apcata.2025.120151
Received 15 November 2024; Received in revised form 24 January 2025; Accepted 31 January 2025
Available online 6 February 2025

formation of an enolate from acetone, which then undergoes a nucleophilic attack on furfural. This is followed by dehydration, leading to the production of an α,β-unsaturated carbonyl compound [26]. These reactions are especially important in biomass conversion, as they allow the creation of complex, energy-dense molecules from simpler, renewable feedstocks [25]. At the industrial scale, aldol condensations are commonly catalyzed by strong alkalis under homogeneous conditions [27]. Processes involving the condensation of furfural and acetone, catalyzed by alkalis like NaOH, are well-documented [21]. The major drawbacks of the homogeneous processes are the potential corrosion of reaction vessels and process equipment, the challenging separation of the products from the reaction mixture, and the high cost derived from the treatment of the process wastewater [19]. To address those problems, the substitution of the homogeneous strong alkali catalysts with heterogeneous solid basic catalysts has been proposed. Heterogeneous solid catalysts can be recovered by simple operations such as filtration or centrifugation in plants based on continuous or batch slurry reactors, while the separation of the catalyst is not an issue in processes based on catalytic packed bed reactors. In addition, the absence of strong alkalis in the liquid phase minimizes the problems related to equipment corrosion and the generation of process wastewater. The use of heterogeneous catalysts, however, poses some challenges as well, since the deactivation of the catalysts, the feasibility of their regeneration and reactivation, and they effective lifespan are critical aspects that must be considered as well. Numerous heterogeneous catalysts have been developed for the aldol condensation of furfural and acetone with significant activity and selectivity towards the C8 and C13 products [22, 28–30], several of those proving to be reusable [22,31]. Catalysts based on hydrotalcites have received considerable attention. Hydrotalcites (HTs) are carbonate minerals classified as layered double hydroxides (LDH) with the general formula $[M^{2+}_{1-x}M^{3+}_{x}(OH)_2]^{x+}\ A^{n-}_{x/n}{\cdot}mH_2O$. In this structure, M^{2+} and M^{3+} represent divalent and trivalent metal ions, while A^{n-} refers to interlayer anions such as carbonates, nitrates, fluoride or chloride [32]. HT materials can be readily synthesized by co-precipitating suitable magnesium and aluminum salts in alkaline media. As-synthesized HTs are used in catalysis because of their mild Brønsted basicity. Conversely, as-synthesized (HTs) are often calcined to form mixed metal oxides (MMOs), also referred to as layered double oxides (LDOs), which are known for their strong Lewis basicity [33]. During calcination, the layers of hydrotalcites (HTs) collapse; however, the layered double hydroxide (LDH) structure is not entirely lost and can potentially be regenerated by immersing the mixed metal oxide (MMO) in an aqueous solution [34]. This approach facilitates the synthesis of hydrotalcite-derived catalysts with various interlayer components, which are known for their strong Brønsted basicity [35]. LDH-derived catalysts have been used in the aldol condensation between hydroxymethyl furfural (HMF) and acetone to produce C9 and C15 compounds. The catalyst's reusability was examined, revealing a decrease in activity after the reaction [26]. Deactivation of Mg-Al hydrotalcite catalysts during aldol condensation can occur due to the formation of carbonaceous deposits, leaching of active components, and structural changes due to sintering. The water produced during the reaction can modify the basicity of the catalyst and strongly adsorb onto its surface. Together, those factors contribute to the catalyst's deactivation over time [36]. The regeneration and the reusability of the spent solid catalysts are critical questions that must be addressed to assess their long-term performance [37]. In this paper we have studied the activity and selectivity of three catalysts derived from a 3:1 Mg:Al hydrotalcite (as-synthesized, calcined, and rehydrated), for the aldol condensation of furfural with acetone on a continuous packed bed reactor operated at high space velocity. The work has focused on the deactivation of the catalysts with the time on stream and has explored the regeneration and reusability of the catalysts after deactivation, a key aspect for scaling up the production of SAF precursors from lignocellulosic biomass.

2. Materials and methods

2.1. Catalyst synthesis

The Mg/Al (3:1) hydrotalcite catalyst (HT) was synthesized by co-precipitation as described in previous studies [38,39]. A solution with the metal precursors was prepared by dissolving 27.6 g of magnesium nitrate hexahydrate (extra pure, Acros Organics) and 13.5 g of aluminum nitrate nonahydrate (≥ 98 %, Fisher Chemical) in 200 mL of deionized water (0.54 $mol{\cdot}L^{-1}$, $Mg(NO_3)_2$ and 0.18 $mol{\cdot}L^{-1}$, $Al(NO_3)_3$). A second solution was prepared by dissolving 20.0 g of sodium hydroxide (98.9 %, Fisher Chemical) and 13.2 g of anhydrous sodium carbonate (≥ 99.5 %, Fisher Chemical) in 250 mL of deionized water (2.0 $mol{\cdot}L^{-1}$ NaOH and 0.5 $mol{\cdot}L^{-1}$ Na_2CO_3). Both solutions were added dropwise (1.5 $mL{\cdot}min^{-1}$) at room temperature into a glass vessel containing 100 mL of deionized water under magnetic stirring at 500 rpm. The pH was monitored using a pH meter (HI-5222, HANNA Instruments) and it was kept at 10 by adjusting the rate of addition of the basic solution. The glass vessel was then covered, and the co-precipitation medium was allowed to stir at room temperature overnight. The resulting solid was separated by vacuum filtration (qualitative filter paper, Fisher Scientific) and subsequently washed with 3 L of deionized water to completely remove sodium ions [40]. The resulting solid was then transferred into a crucible and dried at 80 °C for 24 h. The dried solid was ground, sieved to 300 μm, and stored in a closed vial inside a desiccator. This procedure produced from 10 to 11 g of dry hydrotalcite.

The calcined catalysts (CHT) were prepared by placing dry hydrotalcite in a muffle furnace (HD-150, Hobersal, Spain) at room temperature. The temperature of the furnace was gradually increased to 500 °C and holding this temperature under static air for 3 h. Subsequently, the furnace was allowed to naturally cool down below 150 °C. The crucible was then covered, removed from the furnace, and left to cool down to room temperature in a desiccator. The resulting calcined hydrotalcite (CHT) was sensitive to the moisture and carbon dioxide present in air, which tend to adsorb on the material. Freshly calcined samples were therefore used in all the reactions. The calcination process typically resulted in a mass loss ranging from 40 % to 50 % of the mass of the initial HT. The rehydrated hydrotalcite (RHT) was prepared by suspending ca. 0.6 g of freshly calcined hydrotalcite (CHT) in 30 mL of argon bubbled water at room temperature under stirring at 300 rpm for 24 h [26]. The rehydrated solid was filtered, it was immediately dried at 50 °C under vacuum at 0.07 atm of absolute pressure on a rotary evaporator [40], and it was transferred to the reactor. The samples of the catalysts taken for characterization were stored in sealed 5 mL vials and kept in a desiccator.

Reusability tests of the calcined and rehydrated hydrotalcites were conducted. On those tests, the catalyst was quantitatively recovered from the reactor after each experiment, it was washed with 5 mL of ethanol, and then it was calcined in a muffle furnace using a three-step temperature program. The sample was first heated from room temperature to 250 °C and held two hours, then heated to 350 °C and held one hour, and finally heated to 500 °C and held for two more hours. This procedure resulted on a slow carbonization and burning of the condensation products deposited on the surface of the catalyst and it prevented the overheating of the material due to a fast combustion. Excessive overheating would change the crystalline structure of the calcined material favoring the formation of spinel phases, resulting on a permanent loss of catalytic activity [41]. In the reusability tests of CHT, the recalcined material was subsequently loaded into the reactor and the reaction started immediately. In the case of the rehydrated hydrotalcite (RHT), after calcination the sample was rehydrated as described before and it was immediately transferred to the reactor to start the following reaction cycle.

2.2. Catalyst characterization

The textural properties of the catalysts were determined from their nitrogen physisorption isotherms at 77 K using a Quadrasorb SI Model 4.0 instrument with the QuadraWin Software (Quantachrome Instruments, v. 5.0). The surface area was calculated with the BET model and the pore volume and the pore size distribution with the BJH model. The crystalline structure of the materials was analyzed by X-Ray Diffraction (XRD) with a Bruker-AXS D8-Advance diffractometer. The angular 2θ range was from 5 to 80 degrees. Data were accumulated with an angular step size of 0.02 degrees and a step time of 0.5 s per step. Cu Kα radiation was generated from a copper X-ray tube operating at 40 kV and 40 mA. The crystallite size and lattice strains were calculated with the X'Pert-HighScore Plus software (Malvern Panalytical B.V.) using the Scherrer's equation [42]. Environmental scanning electron microscopy (ESEM) was conducted with a Quanta 600 instrument (FEI Company). Energy Dispersive X-ray Spectroscopy (EDX) analysis was accomplished using an Oxford Instruments EDX detector with an accelerating voltage of 20 kV and a working distance of 10 mm under high vacuum conditions. Micrographs were captured on samples that prior to imaging had been coated with a 15 nm layer of gold using a Q150R ES sputter coater from Quorum Technologies. Field emission scanning electron microscopy (FESEM) was performed on a Scios-2 instrument (ThermoFisher) under high vacuum. Transmission electron microscopy (TEM) images were acquired using a JEOL F200 TEM ColdFEG operated at 200 kV was used for the transmission electron microscopy characterization. TEM images and electron diffraction patterns were acquired with a Gatan OneView camera, a CMOS-based and optical fiber-coupled detector of 4096 by 4096 pixels. Gatan Digital Micrograph program was used to process the (S)TEM images. STEM images (1024 ×1024 pixels) were recorded from the JEOL bright-field (BF) and high-angle annular dark-field (HAADF) detectors with a nominal camera length of 150 mm. Samples were inserted in a JEOL beryllium double-tilt holder for energy dispersive x-ray spectroscopy (EDS). STEM-EDS mapping was recorded from an EDS Centurio detector (silicon drift) with an effective area of 100 mm^2 and 133 eV of energy resolution. STEM-EDS maps (512 ×512 pixels) were processed with the JEOL Analysis software. Fourier-transform infrared spectroscopy (FT-IR) spectra were obtained using an FT/IR 6700 Jasco spectrometer equipped with a TGS detector and an ATR PRO ONE accessory (diamond crystal kit high-throughput model optimized for mid-IR measurements). Each spectrum was recorded by averaging 32 scans at a resolution of 4 cm^{-1} over a wavelength range of 600–4000 cm^{-1}. The basicity of the catalysts was investigated by temperature-programmed desorption of CO_2 (TPD-CO_2) on an AutoChem II 2920 chemisorption analyzer from Micromeritics. Initially, the catalyst samples were dried at 393 K for 100 min under a helium flow rate of 30 sccm. Subsequently, the samples were cooled to 308 K and exposed to a flow of 30 sccm of 2.5 % CO_2 in helium for 30 min. The temperature was then ramped up to 1073 K at a rate of 10 K·min^{-1} under a helium flow of 30 sccm. The desorbed CO_2 was measured using a thermal conductivity detector (TCD). A cold trap containing an ethanol: ethylene glycol mixture (20:80 v:v) at 208 K was placed before the detector to remove water vapor from the gas and avoid its contribution to the TCD response.

2.3. Catalyst activity testing

Testing of the activity and stability of the catalysts for the aldol condensation of furfural and acetone was performed on a continuous flow tubular packed bed reactor. The reactor consisted of a 40 mm long 316 L stainless-steel tube with a 6 mm internal diameter and an 8 mm outer diameter. The reactor was filled with catalyst (c.a. 400 mg) sieved to 100–200 μm, which was contained inside the tube with 2 μm stainless steel frits at both ends. The feed to the reactor was a premixed solution containing a furfural-to-acetone molar ratio of 1:10. The feed was delivered at room temperature by a HPLC pump (Gilson 305) with a flowrate of 0.2 mL·min^{-1}, which corresponds to a furfural weight hourly space velocity (WHSV) of 5.77 h^{-1}. Since furfural undergoes condensation and degradation upon exposure to air and light, freshly distilled furfural was used in each experiment. During the experiments, the feed container was bubbled with a small flow of argon to displace oxygen, and it was kept wrapped with aluminum foil to avoid exposure to light. The reactor was submerged into a silicone oil bath heated to 100 °C with a magnetic stirring plate (IKA RCT standard). All the experiments were performed at that temperature, which was selected based on an earlier study by Tampieri et al. [23] on the effect of reaction temperature with similar catalysts. The pressure in the reactor was maintained at 12 bar(a) with a back-pressure regulator (GO regulators LB1) to avoid the formation of a vapor phase. The catalysts were tested under constant conditions for up to 11 h of time-on-stream, depending on how fast their deactivation was. Samples of the product solution were collected at regular intervals and analyzed by GC-MS and GC-FID.

The reaction products were quantified by gas chromatography using a flame ionization detector (GC-FID, Agilent 6890 N). Hydrogen (30 mL·min^{-1}) was used as the carrier gas with a TRB-5 column (TR-120232, Teknokroma, Spain; 30 m length, 0.25 mm inner diameter and 25 μm film thickness). The temperature program consisted of three steps: a constant temperature of 50 °C for 2 min, followed by a linear temperature ramp from 50 to 300 °C at 40 °C·min^{-1}, and a final constant temperature of 300 °C for 6.75 min. The GC-FID was calibrated with furfural/acetone mixtures having furfural concentrations corresponding to 0, 25, 50 and 75 % conversion. Quantification of the aldol condensation products was based on the furfural calibration curve by using the effective carbon number (ECN) method. This approach relies on the structural similarities of the molecules involved (as they share the same furfural ring), and it was already used in earlier studies on the same reacting system [43]. Identification of the reaction products was conducted by Gas Chromatography-Mass Spectrometry (GC-MS) using an Agilent 6890 with Mass Spectrometer 5973. A HP-5MS column (30 m length, 0.25 mm internal diameter, and 25 μm film thickness) was used with hydrogen as carrier gas (Fig. S1 to S10 and Table S1).

The instantaneous conversion of furfural ($X(t)_{FF}$), the selectivity ($S(t)_j$) and the yield of the products ($Y(t)_j$), and the furan ring balance ($FRB(t)$) were calculated with Eqs. 1 to 4; $c_{FF,0}$ and $c(t)_{FF}$ are the concentrations of furfural in the feed and product streams, respectively, j identifies the different products, ν_j is the number of furan rings in product j, and $c_j(t)$ is the concentration of product j in the reactor effluent at the time on stream t. The density of the liquid was assumed to be independent of the composition. An instantaneous selectivity for the formation of products deposited on the catalyst was estimated from the furan ring balance, according to Eq. 5. The accumulated yield of each product at a time t along an experiment was obtained from Eq. 6, where t_f is the total time on stream of the catalyst in that experiment. When $t = t_f$ Eq. 6 gives the total yield of product j obtained during the entire duration of the experiment. The time integral in Eq. 7 was evaluated by trapezoidal rule since the data points were unevenly spaced. Finally, the overall conversion of furfural (X_{FF}) and the total selectivity to each j product (S_j) were calculated from the total yields, according to Eqs. 7 and 8.

$$X(t)_{FF} = \frac{c_{FF,0} - c(t)_{FF}}{c_{FF,0}} \tag{1}$$

$$S(t)_j = \frac{\nu_j c(t)_j}{c_{FF,0} - c(t)_{FF}} \tag{2}$$

$$Y(t)_j = \frac{\nu_j c(t)_j}{c_{FF,0}} = X(t)_{FF} S(t)_j \tag{3}$$

$$FRB(t) = \frac{1}{c_{FF,0}} \sum_j \left(c(t)_{FF} + \nu_j c(t)_j \right) \tag{4}$$

Table 1
Surface composition determined by EDX analysis and textural properties measured by nitrogen physisorption for the as prepared catalysts, and the spent catalysts after four cycles of activation and reaction.

Catalyst	Composition			Textural properties		
	Mg [wt%]	Al [wt%]	Mg/Al [mol·mol^{-1}]	S_{BET} [m^2·g^{-1}]	V_{pore} [mL·g^{-1}]	r_{pore} [nm]
FHT	20.5	6.6	3.1	123	0.57	6.2
CHT	23.9	7.9	3.0	187	0.97	5.0
Re-CHT−4	22.5	7.6	3.0	181	0.92	5.2
RHT	21.3	7.3	2.9	76	0.29	6.4
Re-RHT−4	21.1	7.2	2.9	64	0.27	6.0

$$S(t)_{DP} = \frac{1 - FRB(t)}{c_{FF,0} - c(t)_{FF}} \quad (5)$$

$$Y_j = \frac{1}{t_f}\int_0^t Y(t)_j dt \quad (6)$$

$$X_{FF} = \sum_j Y_j \quad (7)$$

$$S_j = \frac{Y_j}{X_{FF}} \quad (8)$$

To test the reusability of the catalysts, samples of CHT and RHT were subjected to four consecutive cycles of activation and reaction. The spent catalysts after the fourth reaction tests were labelled Re-CHT-4 and Re-RHT-4 and were stored under nitrogen in closed vials for further characterization.

3. Results and discussion

3.1. Characterization of the as-prepared catalysts

The elemental composition of the material's surface was tested by EDX (Table 1, Fig. S11). The content of magnesium and aluminum varied according to the changes in oxygen and carbon, but the Mg/Al atomic ratio was constant at the intended value of 3.0 ± 0.1. Sodium was not detected in FHT, indicating a successful washing of the HT catalyst. The textural properties of the catalysts were determined by nitrogen physisorption (Fig. 1). All the materials had type IV isotherms according to the IUPAC classification [44] with hysteresis lops of the type H4, which are characteristics of porous materials formed by aggregates of parallel laminar structures. The FHT had a surface area of 123 m^2·g^{-1} with a pore volume of 0.57 mL·g^{-1} and an average pore radius of 6.2 nm. Calcination led to a more pronounced hysteresis loop in CHT by an increase in porosity, which gave higher surface area and the pore volume, but decreased the average pore size (Table 1). On the contrary, rehydration (RHT) caused a reduction in surface area (76 m^2·g^{-1}) and pore volume (0.29 mL·g^{-1}), well below the values of the as-synthesized hydrotalcite although the pore radius (6.4 nm) was equivalent. The differences in surface area and pore volume are related to the presence of large anions such as carbonates and nitrates in the interlayer spaces of FHT, which are less abundant after calcination and rehydration.

The structure of the as-synthesized materials was investigated by powder X-ray diffraction. FHT had the typical diffractogram of a hydrotalcite structure (Fig. 2), with signals at 11.36°, 22.88°, 34.71°, 39.11°, 46.36°, 60.54° and 61.84° (JCPDS 00–022–0700). Those peaks correspond to sharp reflections from the (003), (006), (009), (110) and (113) crystallographic planes, with two broader peaks at (015) and (018). The diffractogram of the calcined hydrotalcite (CHT), identified with JCPDS 00–004–0829, showed peaks at 43.29° and 62.76°. Calcination of the FHT caused the collapse of the layered double hydroxide structure into a mixed oxide phase, Mg(Al)O_x. The calcined sample showed two broad diffraction lines at (200) and (220), corresponding to the cubic phase of periclase [34]. The XRD analysis of RHT confirmed that rehydration triggered the reconstruction of the layered double hydroxide structure of the fresh hydrotalcite, but the crystallite sizes were larger than in the as prepared hydrotalcite indicating an agglomeration of the layers (Table 2). This is consistent with the smaller pore volume

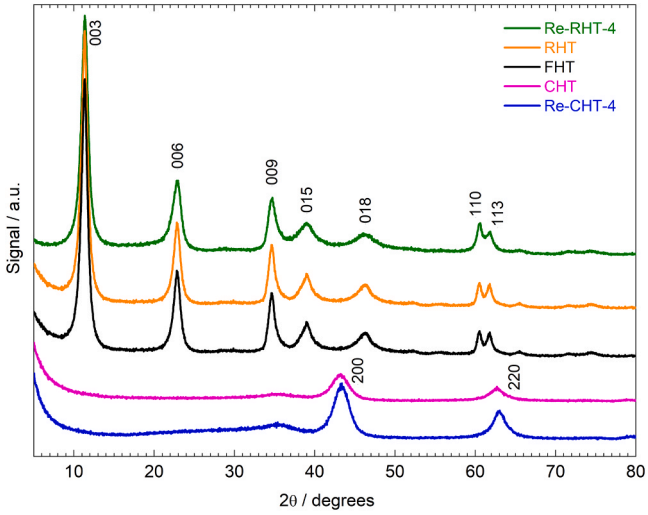

Fig. 2. Powder XRD diffractograms of the as-prepared (FHT), the calcined (CHT) and the rehydrated (RHT) hydrotalcites, and the calcined (Re-CHT-3) and rehydrated (Re-RHT-3) materials after the 4th cycle of reaction and regeneration.

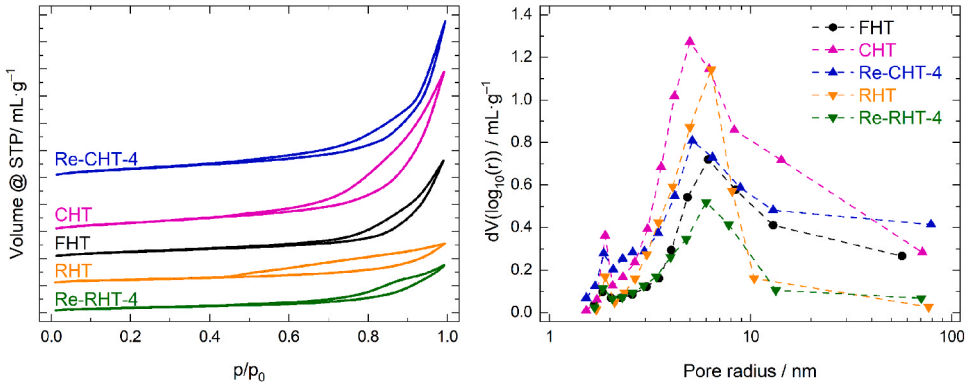

Fig. 1. Nitrogen adsorption-desorption isotherms of the solid catalysts (left) and pore size distributions calculated with the BJH model (right).

Table 2
Crystallite sizes of the as prepared catalysts and the spent catalysts after four cycles of activation and reaction, determined by powder XRD.

Catalyst	2θ [°]	(hkl)	Size [nm]
FHT	11.4	(003)	8.8
	60.5	(110)	16.1
CHT	43.2	(200)	3.6
Re-CHT−4	43.2	(200)	3.9
RHT	11.4	(003)	9.7
	60.8	(110)	19.0
Re-RHT−4	11.4	(003)	8.1
	60.6	(110)	14.8

and surface area explained above. ESEM imaging of FHT (Fig. 3) revealed the desert rose-like aggregates characteristic of the layered double hydroxides, with sheet structures that are stacked together [41]. Calcination increased the roughness of the surface but the apparent morphology of FHT was maintained, which is usual in the mixed oxides formed by collapse of the layered structure of the hydrotalcites. The rehydrated hydrotalcite recovered the layered structure of the hydrotalcite, but the surface appeared to be composed of larger sheets. TEM images show a dense aggregation of plate structures in FHT (Fig. 3). Calcination modified the structure significantly, which was formed by irregular plates embedded in less organized material. Finally, the rehydration of the calcined material recovered the arrangement of dense plates present in RHT.

The Fourier Transform Infrared Spectroscopy (FT-IR) analysis of the as-prepared samples (Fig. 4) agreed with previously reported spectra for this type of materials [39,41,45]. Bands in the range of 600–800 cm^{-1} were attributed to metal-oxygen (Mg-O and Al-O) vibrations in the hydrotalcite structure [26]. Strong absorption bands were observed at ca. 1350–1450 cm^{-1} in FHT and RHT attributed to the asymmetric stretching vibrations of the carbonate anions [40,41,46,47]. The band near 1650 cm^{-1} corresponded to the bending vibrations of water molecules, and the broad band around 3400–3600 cm^{-1} was associated with the stretching vibrations of hydrogen-bonded hydroxy groups in the brucite-like layers, and interlayer water molecules [48]. Those bands were not present in the calcined material (CHT), showing that water had been removed from the interlayer spaces during calcination and that rehydration by exposure of the samples to ambient air during storage and handling was prevented. A broad band at 1450 cm^{-1} was still present in CHT, corresponding to carbonates that were not decomposed completely during the calcination of the hydrotalcite, even if the hydrotalcite structure was destroyed [40,41]. Carbonates in the rehydrated hydrotalcite (RHT) may therefore came from two sources. On the one hand, those that were not completely decomposed during calcination and, on the other hand, those formed by contact with carbon dioxide from the ambient air that transformed interlayer hydroxyls to carbonates as charge-compensating anions in the hydrotalcite structure.

The density and strength of the basic sites of the catalysts were measured by temperature programmed desorption of carbon dioxide (CO_2-TPD). FHT had a large desorption peak at 400 °C, characteristic of the formation of bicarbonate and bidentate carbonate adsorbed species on weak basic sites (Fig. 5). Deconvolution of the adsorption peak revealed a secondary peak at 558 °C, attributed to monodentate carbonate species adsorbed on strong basic sites. The total basicity of the sample was 1.86 $mmol_{CO2} \cdot g^{-1}$, with 8.5 % corresponding to the strong basic sites (Table 3). The basicity of the calcined hydrotalcite was very low when compared to the fresh hydrotalcite. Calcination removed interlamellar water and the hydroxyl groups responsible for the weak basicity sites, and the peak at 400 °C was completely suppressed in CHT. The total basicity was 0.20 $mmol_{CO2} \cdot g^{-1}$. Deconvolution of the signal

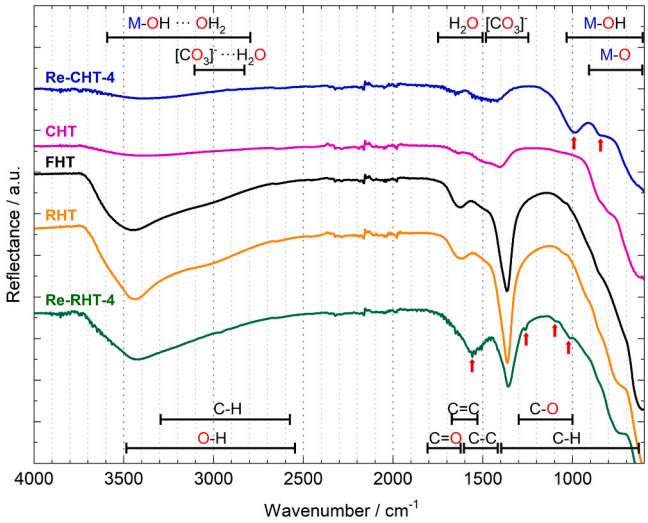

Fig. 4. FT-IR spectra of the as-prepared (FHT), the calcined (CHT) and the rehydrated (RHT) hydrotalcites, and the calcined (Re-CHT-3) and rehydrated (Re-RHT-3) materials after the 4th cycle of reaction and regeneration.

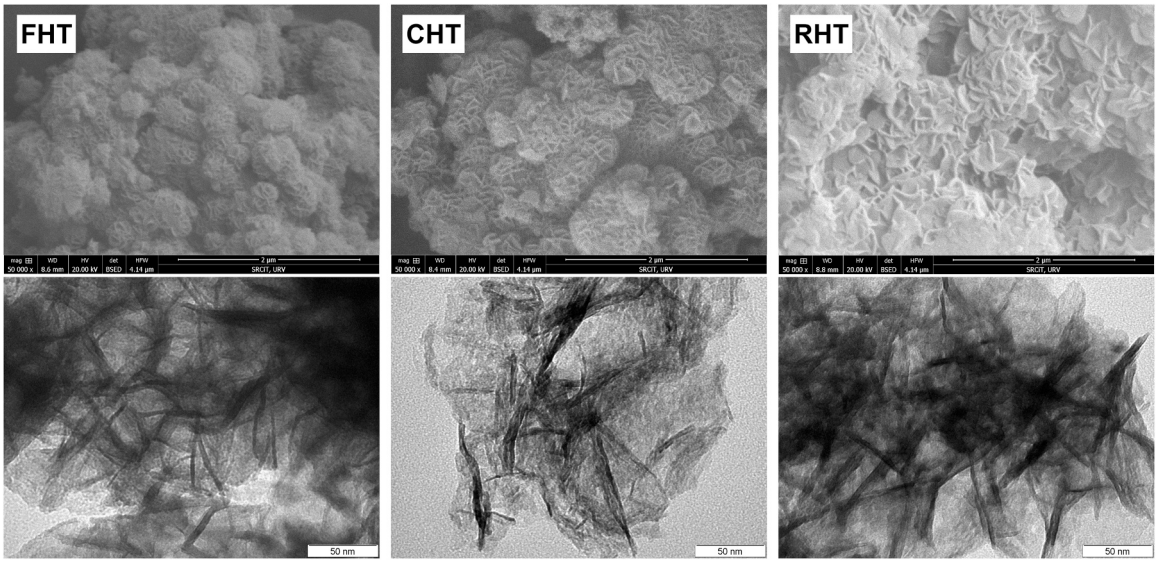

Fig. 3. ESEM (top) and TEM (bottom) images of the as-prepared (FHT), the calcined (CHT) and the rehydrated (RHT) hydrotalcites.

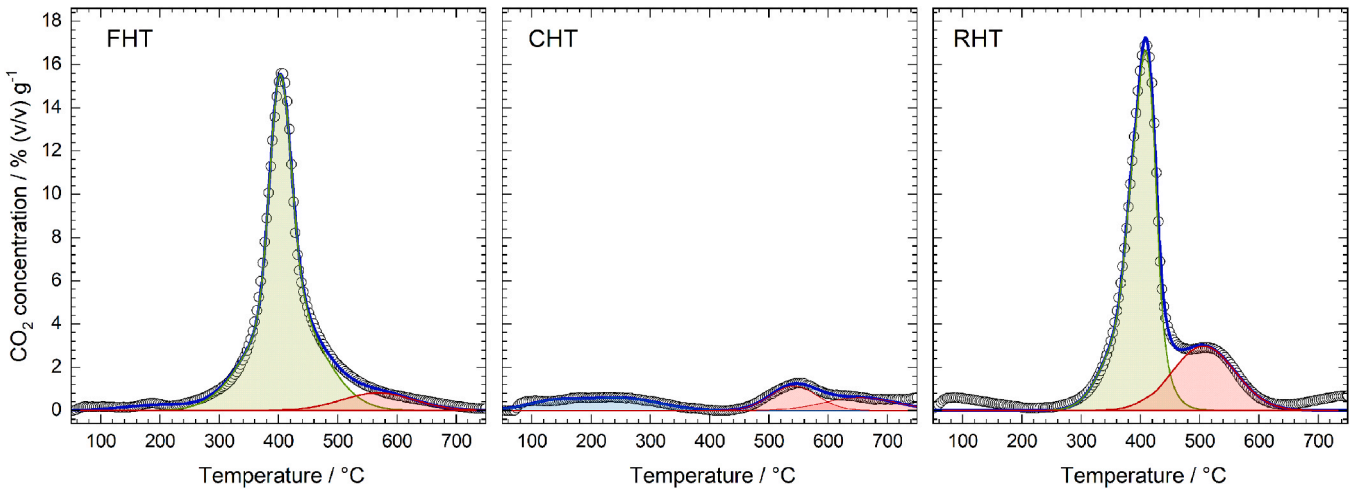

Fig. 5. CO_2-TPD profiles of the as-prepared (FHT), the calcined (CHT) and the rehydrated (RHT) hydrotalcites.

Table 3
Quantification of the CO_2-TPD profiles for the as prepared catalysts.

	Weak sites		Strong sites		Strong sites	
Catalyst	Peak at [°C]	CO_2 evolved [mmol/g]	Peak at [°C]	CO_2 evolved [mmol/g]	Peak at [°C]	CO_2 evolved [mmol/g]
FHT	400	1.61	558	0.15	-	-
CHT	-	-	533	0.15	644	0.05
RHT	410	1.34	510	0.52	-	-

revealed two peaks of strong basicity, one at 533 °C combined with a smaller one centered at 644 °C. The latter accounted for 25 % of the basicity and corresponded to stronger basic sites created on low-coordination oxygen anions located at the edges of the platelets of the mixed metal oxides, which were not present on FHT. After rehydration (RHT) the material recovered the hydrotalcite structure and the weak strength sites were again the most abundant, with a peak at 410 °C. The total basicity was 1.86 $mmol_{CO2} \cdot g^{-1}$ and a larger superimposed peak at 510 °C of strong basic sites was present, that accounted for 28 % of the total basicity.

3.2. Activity of the as-prepared catalysts

The as synthesized (FHT), the calcined (CHT) and the rehydrated (RHT) hydrotalcites were tested for the aldol condensation of furfural and acetone at 100 °C using a furfural WHSV of 5.77 h^{-1} with a pre-mixed feed having a furfural-to-acetone molar ratio of 1:10. The as synthesized hydrotalcite had low catalytic activity. The instantaneous conversion of furfural was only 65.8 % at the beginning of the experiment (Fig. 6 and Table S2). The only products detected were (*E*)-4-(furan-2-yl)but-3-en-2-on (C8) and (1*E*,4*E*)-1,5-di(furan-2-yl)penta-1,4-dien-3-one (C13), with a respective selectivity of 26.2 % and 11.0 %. The instantaneous conversion of furfural and the selectivity to C8 and C13 dropped continuously with the time-on-stream (TOS). After 4.5 h, furfural conversion was only 6.35 % and selectivity was 2.57 % for C8 and 1.33 % for C13. The balance of furan rings (FRB, Eq. 4) was 58.6 % at the beginning of the experiment, which implies that 41.4 % of the furfural fed to the reactor was converted to products that were retained in the packed bed (DP). The FRB improved as the catalyst deactivated, showing that the formation of DP was induced by the catalyst itself and was not related to homogeneous reactions in the liquid phase. Even if the conversion of furfural and the selectivity to C8 and C13 decreased with the TOS, the selectivity to DP grew (calculated from the FRB, Eq. 5). DP was produced preferentially instead of C8 and C13 from the start of the reaction. Consequently, the accumulated yields of C8 and C13 plateaued after 3 h of TOS while that of DP continued to grow. The deposited products were adsorbed only on the surface of the catalyst, which was covered with a light-brown layer of material after the reaction (Fig. S12). The inner walls of the reactor tube and the porous metal

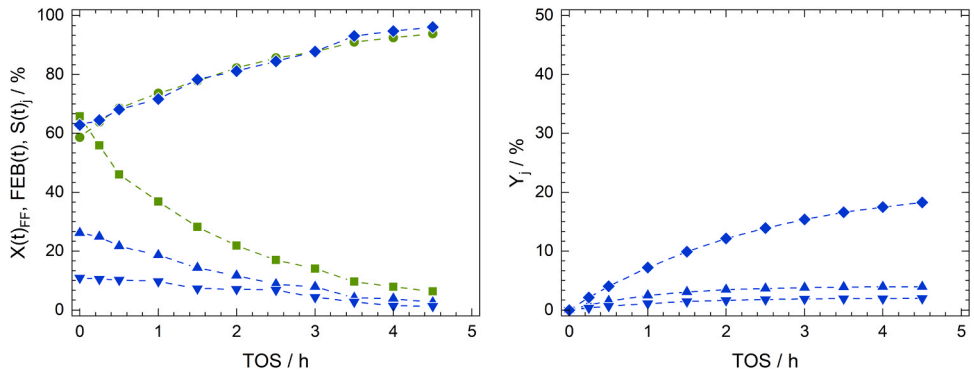

Fig. 6. Activity of the as prepared hydrotalcite (FHT): instantaneous furfural conversion (■), furan rings balance (●) and selectivity (left) and accumulated yields of the products (right) with TOS. (C8 ▲; C13 ▼; DP ◆; the dashed lines only indicate trends).

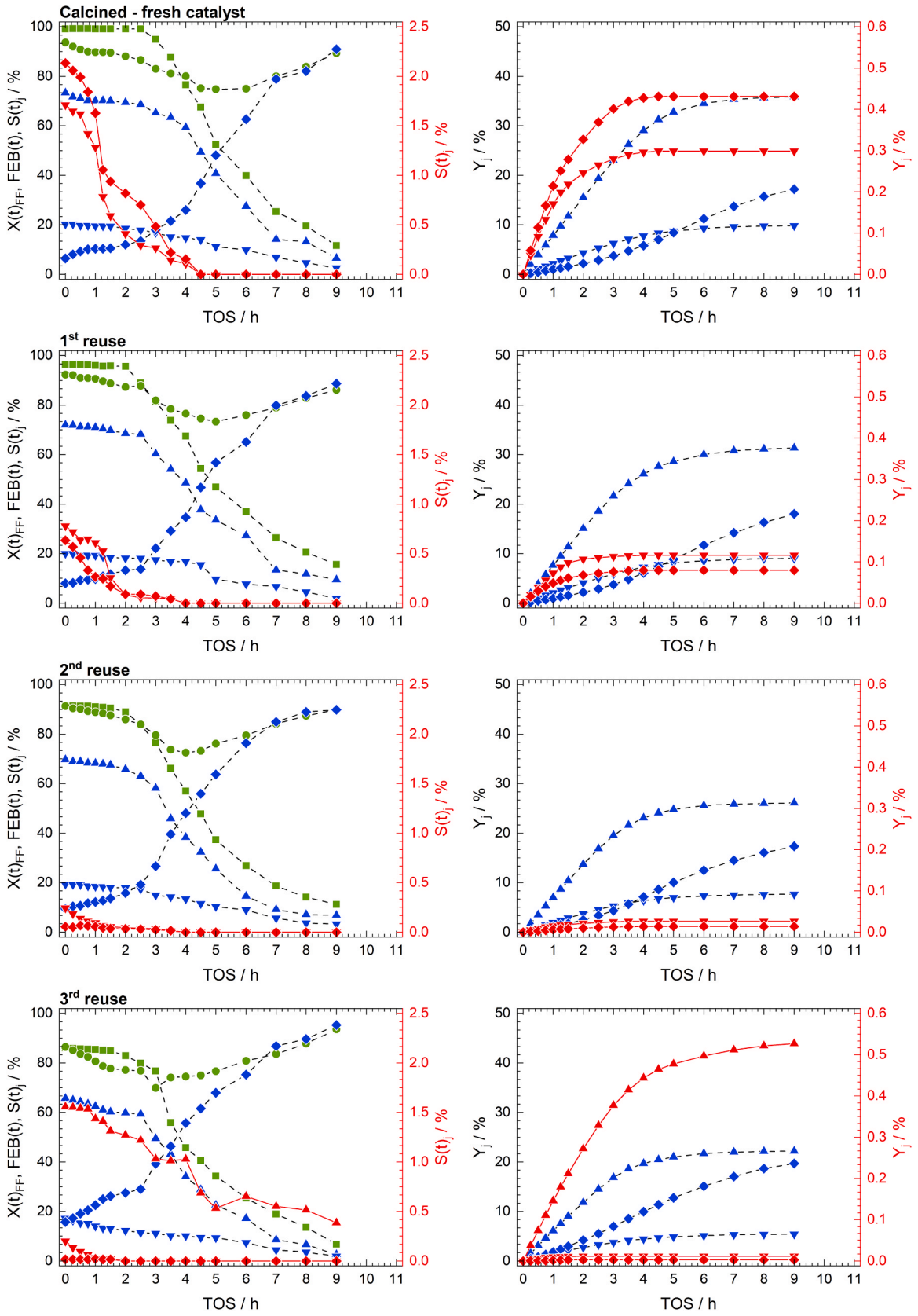

Fig. 7. Activity of the as prepared CHT catalyst (top) and the regenerated and reused CHT: instantaneous furfural conversion (■), furan rings balance (●) and selectivity (left) and accumulated yield of products (right) with TOS. (C8 ▲; C13 ▼; DP ◆; C8OH ▲; C16 ▼; C21 ◆; the dashed lines only indicate trends).

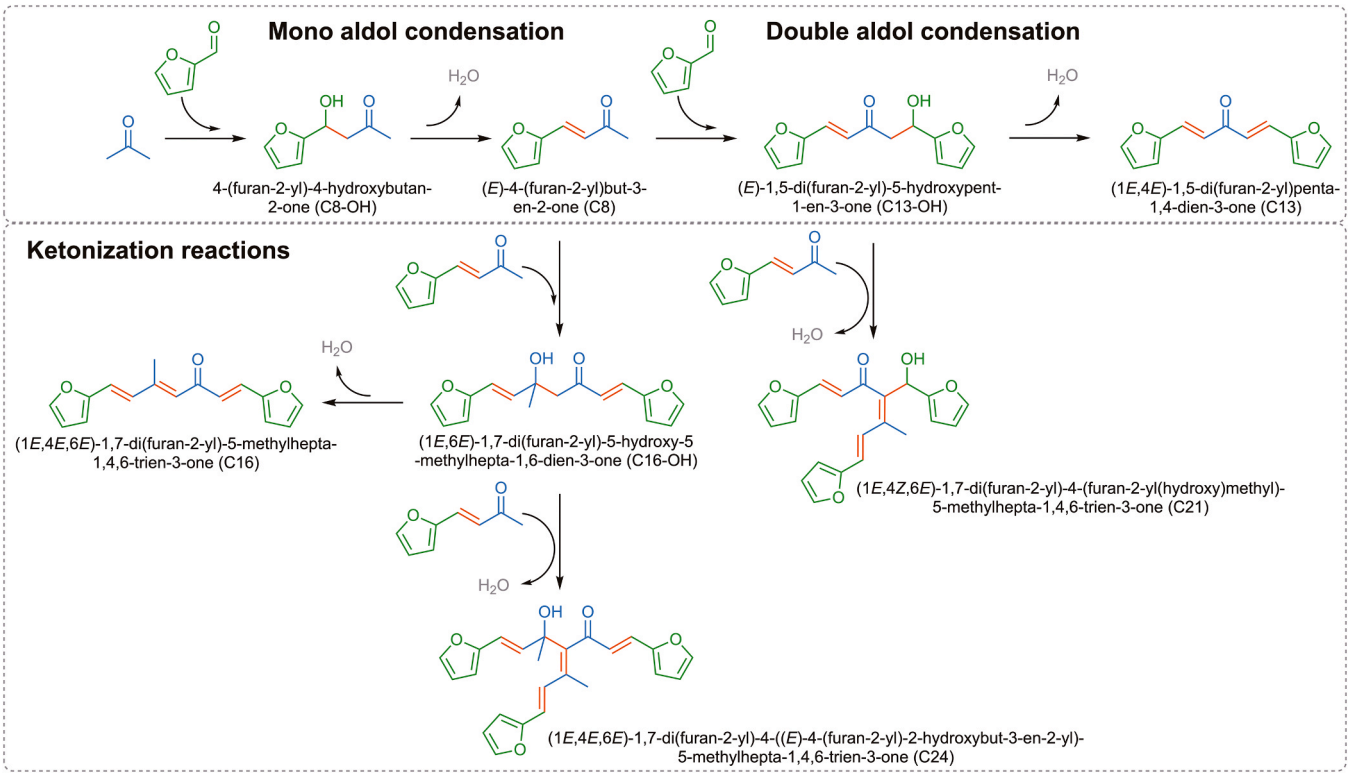

Fig. 8. Simplified reaction pathways for the aldol condensation of furfural and acetone and the secondary ketonization reactions that form the low-solubility products.

plates holding the catalyst were clean and had no attached deposits. A test pumping pure acetone at 100 °C and 12 bar(a) through the packed bed of spent catalyst after the reaction showed that the material deposited on the catalyst was insoluble in hot acetone. The limited catalytic activity of FHT was explained by a low content of strong basic sites in this material. In fact, FHT would have fewer free basic sites than those measured by CO_2-TPD. The strong sites determined from the desorption measurement were mostly due to the carbonates trapped in the interlamellar spaces of the double layered structure during the synthesis of the hydrotalcite, which would decompose as temperature exceeded 500 °C during the CO_2-TPD analysis. Those carbonates would compensate part of the strong basic sites of the catalyst and decrease the number of the sites active for aldol condensation.

The calcined hydrotalcite (CHT) was more active than the as synthesized hydrotalcite. The instantaneous furfural conversion was 99.2 % at the beginning of the experiment and remained stable for more than two hours (Fig. 7 and Table S3). During this initial stage the selectivity to C8 and C13 tended to stabilize at ca. 70 % and 19 %, respectively, the FRB was close to 90 % and the selectivity to DP was around 10 %. At 2.5 h of TOS the conversion of furfural dropped gradually to a value of 11.6 % after 9 h. The selectivity to C8 and C13 followed a decreasing trend, and the selectivity to DP grew steadily to a 90.9 % after 9 h. Small concentrations of diacetone alcohol and mesityl oxide formed by the self-ketonization of acetone were observed, together with two compounds that did not appear with the FHT catalyst. They were identified by GC-MS (Fig. S9 and S10) as (1E,4E,6E)-1,7-di(furan-2-yl)-5-methylhepta-1,4,6-trien-3-one (C16) and (1E,4Z,6E)-1,7-di(furan-2-yl)-4-(furan-2-yl(hydroxy)methyl)-5-methylhepta-1,4,6-trien-3-one (C21). The first was formed by the ketonization of two units of C8 as shown in the simplified reaction pathway in Fig. 8, and C21 resulted from the ketonization of C13 with C8. The respective initial selectivity of C16 and C21 were 1.71 % and 2.13 %, but their concentration diminished rapidly and were not detected after 4 h. The suppression of the formation of C16 and C21 concurred with the stagnation of the accumulated yields of C8 and C13 and an acceleration on the rate of grow of the yield of DP. The rehydrated hydrotalcite (RHT) had superior activity than the calcined and the as synthesized hydrotalcites. Furfural conversion was higher than 99 % during the initial four hours (Fig. 9 and Table S4) and the deactivation rate was slow, while the FRB started at 98.1 % and it dropped gradually to 90.5 %. The selectivity to C8 and C13 also decreased slowly, as did those of the trace products C16 and C21 that were below 1 % at the start of the experiment. Furfural conversion and selectivity to C8 and C13 dropped fast after 4 h and the formation of DP grew accordingly. The accumulated yields increased linearly during the first four hours, with DP having the lower rate of grow, but after that the yields of C8, C13, C16 and C21 tended to stabilize while the formation of DP accelerated. Overall, RHT was more selective to C8 than CHT, and had a similar selectivity to C13. The final yield of C8 after 11 h of TOS was higher than that with the CHT after 9 h. The deactivation of the three catalysts was caused by the deposition of organic products on their surface. Given their insolubility in acetone, the deposited compounds probably consisted of large oligomers formed by ketol oligomerization reactions [49,50]. The presence of minor amounts of C16 and C21 among the reaction products with CHT and RHT supports the hypothesis of a deactivation caused by the formation of insoluble species by oligomerization on the active sites of the surface. This would block the active sites of the catalyst over time, thus diminishing its capacity to form C8 by enolization between furfural and acetone, while it would consume C8 in situ to form larger oligomers that remained attached to the surface.

3.3. *Reusability of CHT and RHT*

Given their rapid deactivation, the regeneration and reuse of CHT and RHT was investigated. Both catalysts were reactivated by controlled calcination to remove the organic deposits, and in the case of RHT the recalcined material was rehydrated as described in the experimental section. Three consecutive reactivation and reuse tests were conducted

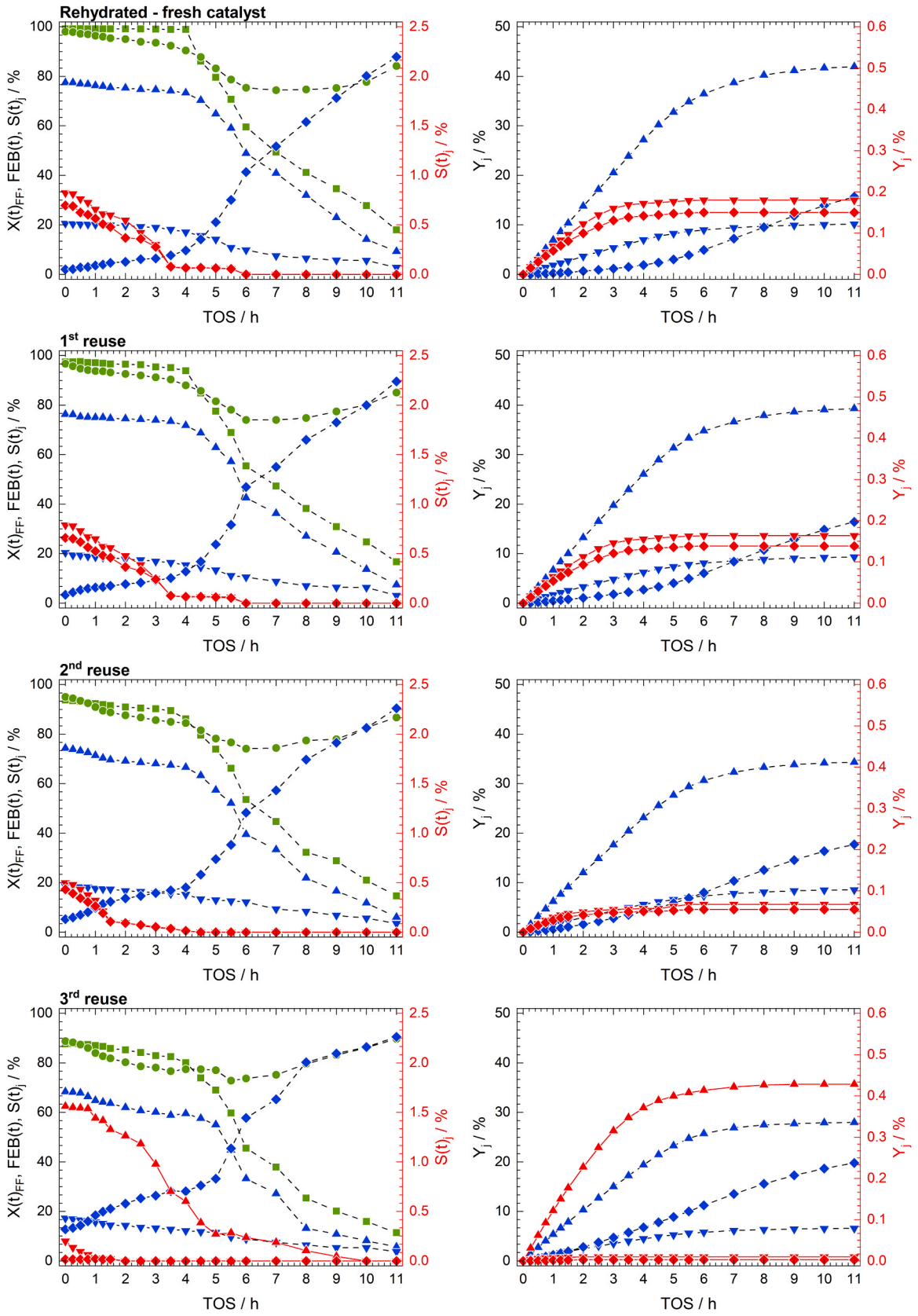

Fig. 9. Activity of the as prepared RHT catalyst (top) and the regenerated and reused RHT: instantaneous furfural conversion (■), furan rings balance (●) and selectivity (left) and accumulated yield of products (right) with TOS. (C8 ▲; C13 ▼; DP ◆; C8OH ▲; C16 ▼; C21 ◆; the dashed lines only indicate trends).

Table 4
Total conversion of furfural and overall selectivity achieved after 9 h of time-on-stream for the as-prepared and reactivated CHT and RHT catalysts, calculated according to Eqs. 7 and 8 (n.d. = not detected).

	Calcined hydrotalcite (CHT)				Rehydrated hydrotalcite (RHT)			
(%)	As prepared	1st reuse	2nd reuse	3rd reuse	As prepared	1st reuse	2nd reuse	3rd reuse
X_{FF}	63.6	58.6	51.2	47.8	63.2	60.9	56.9	51.9
S_{C8}	56.4	53.5	51.0	46.4	65.1	63.4	59.5	53.4
S_{C13}	15.4	15.4	15.0	11.3	15.7	14.9	14.7	12.4
S_{DP}	27.0	30.8	33.9	41.1	18.7	21.2	25.6	33.3
S_{C8OH}	n.d.	n.d.	n.d.	1.10	n.d.	n.d.	n.d.	0.825
S_{C16}	0.469	0.198	0.0512	0.0242	0.284	0.268	0.118	0.0186
S_{C21}	0.678	0.136	0.0267	0.00601	0.237	0.227	0.0963	0.00464

after the first run with each catalyst. In the first reuse test the regenerated CHT was slightly less active than the fresh CHT. The evolution of the product selectivity was qualitatively similar in both cases, but conversion started to drop after only 2 h of TOS instead of 2.5 h in the fresh CHT. The initial selectivity to C16 and C21 was also significantly lower (Fig. 7 and Table S3). The accumulated yields at the end of the experiment were smaller for C8 (31.3 % vs. 35.9 % in the fresh CHT) and C13 (9.03 % vs. 9.82 %), while the yield of DP raised from 17.2 % in CHT to 18.1 % in the first reuse. Successive reactivation treatments resulted on an added loss of activity and selectivity to C8 and C13. In the third reuse the initial conversion was only 86.1 % and the period of quasi-stability only lasted 1.5 h. The selectivity to C8 and C13 dropped faster, and the final yields were significantly lower than in the previous tests while the yield of DP grew accordingly. In addition, only minor amounts of C16 and C21 were seen at the beginning of the run, and they were not detected after 1.5 h of TOS. In contrast with the precedent tests, 4-(furan-2-yl)-4-hydroxybutan-2-one (C8-OH) was present in the products, with a selectivity dropping from 1.56 % to 0.39 % along the run. The reduction in selectivity to C8 and C13 and the grow in DP were explained by a loss of the capacity of the active sites to dehydrate C8-OH to C8, which may favor its ketonization to DP. Finally, the water formed during the aldol condensation and ketonization reactions in CHT could hydrate the catalyst and make the $Mg(Al)O_x$ mixed oxide phase to revert back to the original hydrotalcite structure. However, the formation of the HT structure was not observed by XRD on the catalyst during the third reuse experiment (Re-CHT-4, Fig. 2) because not enough oxides were reverted during the duration of the experiment due to the fast deactivation by the deposition of organic products.

The reusability tests of RHT were conducted during 11 h per cycle (Fig. 9 and Table S4). During the first reuse test, the catalyst gave results that were almost identical to those of the fresh RHT, although the conversion of furfural during the first 4 h and the final yield of C8 were slightly lower. The loss of performance was significant during the second reuse test. Furfural conversion started at just 93.8 % and the initial selectivity to DP during the first 4 h was higher than in the first two uses, thus lowering the yields of C8 and C13. The activity test during the third reuse gave the worst results, with lower selectivity and yields of C8 and C13 than in the anterior cycle. The formation of C16 and C21 was almost suppressed entirely, and a significant amount of C8-OH was detected at the beginning of the test (1.56 % selectivity). The final accumulated yields of C8 and C13 after 11 h were 28.0 and 6.59 % respectively, well below the values of 42.0 % and 10.2 % of the RHT, while the yields of DP were 19.8 % in Re-RHT-3 and 15.7 % in RHT. The total conversion of furfural and the overall selectivity to C13 (c.a. 63 % and 13 %) were almost identical in the as prepared CHT and RHT after the 9 h of TOS (Table 4), but the selectivity to C8 was higher in RHT (65.1 % vs. 56.4 % in CHT) and the selectivity to the oligomerization and the deposition products were markedly lower. Upon reactivation and reuse, RHT

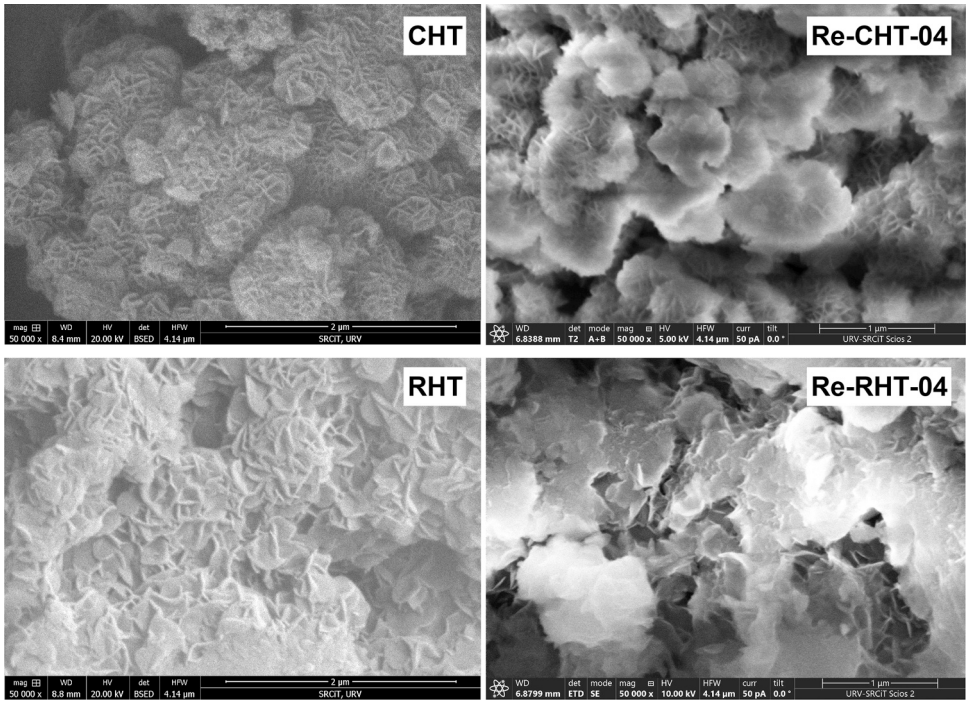

Fig. 10. Scanning electron microscopy images at a magnification of 5×10^4 of the as prepared CHT and spent Re-CHT-4 (top), and the as prepared RHT spent Re-RHT-4 (bottom). (The as prepared materials are ESEM images, the reused materials are FESEM images).

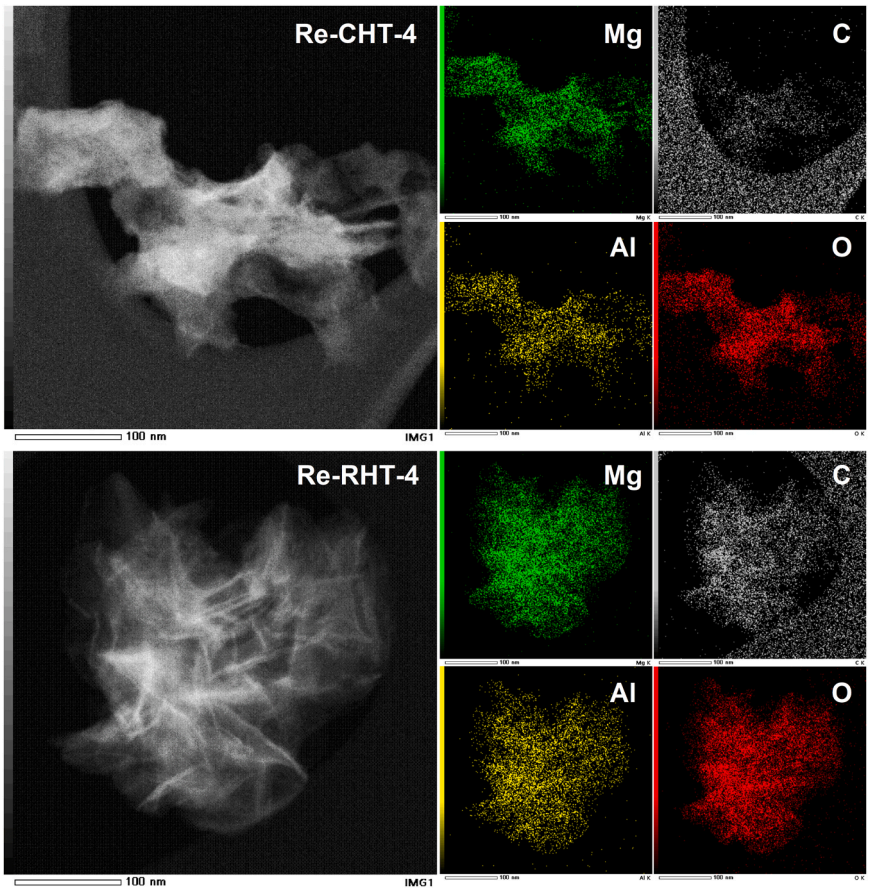

Fig. 11. FETEM and EDX mapping of the spent catalysts: Re-CHT-4 (top) and Re-RHT-4 (bottom).

always outperformed CHT and it was more selective to C8 and less selective to DP while the selectivity to C13 was equivalent. Furthermore, the loss in activity and selectivity between reactivation treatments in RHT was also less pronounced than in CHT after the same number of reactivation treatments.

Two factors should be considered to explain the loss of activity and selectivity after each activation and reaction cycle. The gradual loss of activity of the catalysts could be due, at least partially, to the limitations of our experimental procedure. The calcination, and eventual rehydration of the spent catalysts was not performed in the reactor tube itself. Even if particular care was taken to transfer the catalyst samples quantitatively during the operations involved (emptying the reactor, calcination, rehydration when needed, etc.), small losses were unavoidable. We estimated that from 4 % to 6 % of the original mass of particles was lost after the four cycles of activation and reaction. However, this does not explain the shift in product selectivity with each reuse of the catalysts which can only be attributed to structural changes upon reactivation. Samples of the spent catalysts at the end of the fourth cycle of activation and reaction (Re-CHT-4 and Re-RHT-4) were investigated without performing any additional treatment. The formation of dense aggregates of deposited material on top of the spent catalysts was observed by scanning electron microscopy in both materials (Fig. 10), and the presence of carbon on the fine structure of the catalyst detected by FETEM-EDX (Fig. 11); even if the carbon imaging also showed the contribution of the support grid, the particles sampled were mostly placed on grid voids and the contribution of the carbon located on the catalyst particles was clearly observed. The surface area and the pore volume of both spent catalysts were lower than in their original as prepared forms (Table 1). The average pore radius did not change in Re-CHT-4, but it decreased in Re-RHT-4. The hysteresis loops of the isotherms were significantly smaller in the spent catalysts due to the deposition of organic material inside the porous structure. FTIR analysis of Re-CHT-4 revealed the same small bands related to carbonates, hydroxyls and water than in CHT, but two new bands at ca. 1000 and 850 cm^{-1} were observed (Fig. 4). They were attributed to the C-O and C-H stretching of the deposited organic compounds and were not assigned to the presence of hydroxy groups attached to the metals (M-OH), since no change was detected in the 3400–3600 cm^{-1} region of the hydrogen-bonded hydroxy groups when compared with the spectra of CHT. In the case of Re-RHT-4, a new band at 1550 cm^{-1} which was not present in RHT or FHT was attributed to C═C and C-C bonds of the deposited organics, and weak signals at 1000, 1200 and 1280 cm^{-1} could be related to the C-O stretching. Noticeably, the band at 1550 cm^{-1} was not present in Re-CHT-4, and the signal at 1000 cm^{-1} in the latter was extremely weak in the spent rehydrated catalyst. Those differences between Re-CHT-4 and Re-RHT-4 show that the dominant functionalities of the deposited organic materials may differ in both catalysts. It seemed that the rehydrated catalyst promoted the deposition of more unsaturated oligomers than the calcined catalyst, which would be consistent with its larger content of strong basic sites. However, the catalytic activity of CHT was close to that of RHT, even if the number of strong basic sites was less than half. CHT had a larger surface area and smaller crystallite sizes. The larger surface area made the active sites more available to the reactants, and the smaller crystallite sizes of the Mg(Al)O_x mixed oxides exposed more low-coordination oxygen anions located at the edges of the crystallites, which are more accessible and active to catalyze the aldol condensation reactions. Characterization of the spent catalysts by XRD revealed some structural changes (Fig. 2). The signals of the diffraction peaks of planes (200) and (220) in Re-CHT-4 were higher than in the original CHT pointing to an increase in crystallite size, even if the average size only grew from 3.6 to 3.9 nm (Table 2). Larger crystallites imply less low-coordination oxygen anions exposed at the

edges of the crystallites, thus reducing the number of accessible active sites per unit mass of catalyst. Increased sintering due to the repeated treatments of calcination and reaction could be a plausible reason of the loss of activity and selectivity of the CHT. Regarding the rehydrated hydrotalcite, the diffraction peaks in Re-RHT-4 were wider and less defined than in the as prepared RHT and the crystallinity was actually lower, although the diffractogram only displayed the characteristics signals of the HT structure. The deactivation of CHT and RHT upon reuse could then arise from several factors. One possibility is that not all the oligomeric material deposited during the reactions was burned-off by recalcination at 500 °C, thus accumulating carbonaceous deposits that blocked a growing fraction of active sites with each reuse. A more likely possibility comes from the formation of a spinel phase on the surface of the catalyst during the combustion of the deposited organic material [37,51]. Even if a gradual increase on the temperature of the furnace was used, the occurrence of hotspots on the surface of the catalysts due to a rapid combustion of the organic materials was likely. Those hotspots would promote the formation of spinel phase on top of the $Mg(Al)O_x$ oxides. The amount of spinel was not large enough to be detected by XRD after the third reuse treatment, but it could produce the apparent sintering of the CHT and would also reduce the activity of RHT because the spinel does not revert to the original hydrotalcite upon rehydration.

4. Conclusions

The performance of Mg-Al hydrotalcite catalysts with a Mg:Al atomic ratio of 3:1 has been assessed for the aldol condensation of furfural with acetone. The catalyst has been evaluated at 100 °C on a continuous packed-bed reactor in its as-prepared (FHT), calcined (CHT) and rehydrated (RHT) forms. The main product was C8, which dominated over C13 due to the excess of acetone that was used (acetone:furfural molar ratio of 10:1). Minor amounts of the oligomeric products formed by ketonization of two C8 units to C16, and between one C8 and one C13 to C21 were detected as well. The activity of the catalysts was related to their content of strong basic sites. FHT had the lowest activity due to the reduced number of strong sites and the presence of carbonates in the intralamellar spaces of the hydrotalcite, which partially compensated the existing active sites. CHT had less strong basic sites, but its activity was improved by the higher surface area and the small crystallite sizes, which maximized accessibility. RHT had a slightly better performance than CHT in terms of the yields of C8 and C13 and the stability along the time on stream. Both CHT and RHT, however, deactivated after a few hours of operation. In both cases the deactivation was produced by the deposition of low-solubility oligomer products formed by ketonization. The products covered the catalyst surface and filled the porous structure of the material. In CHT, the water formed as reaction product could influence the deactivation as well, since it could induce a reversion of the $Mg(Al)O_x$ mixed oxides to the hydrotalcite structure. The reusability tests of CHT and FHT revealed a gradual loss on activity and selectivity after each reactivation treatment. This phenomenon was likely produced by the formation of small amounts of spinel due to hotspots on the surface of the catalyst during the recalcination treatments. However, no definitive proof was obtained from the characterization of the spent catalysts.

CRediT authorship contribution statement

Daniel Montane: Writing – review & editing, Visualization, Validation, Data curation. **Constantí Magdalena:** Writing – review & editing, Validation, Supervision. **Medina Francesc:** Writing – review & editing, Supervision, Funding acquisition, Formal analysis, Conceptualization. **Munir Saleem:** Writing – original draft, Investigation, Formal analysis, Data curation.

Declaration of Competing Interest

The authors declare that they have no known competing financial interests or personal relationships that could have appeared to influence the work reported in this paper.

Acknowledgements

This research was supported by the grants PID2021-123665OB-I00 funded by MCIN/AEI/10.13039/50110001103 and “ERDF A way of making Europe”, TED2021-129343B-I00 funded by MCIN/AEI/10.13039/50110001103 and by the “European Union Next-Generation EU/PRTR”, and by the project 2023 CLIMA 00076 funded by AGAUR (Departament de recerca i universitats, Departament d’acció climàtica, alimentació i agenda rural, i el Fons climàtic de la Generalitat de Catalunya). Saleem Munir is grateful for the Ph.D. scholarship “PRE2019-090395”, funded by the Spanish Ministry of Science, Innovation and Universities. The authors are grateful to Dr. Anton Dafinov for his technical assistance on the CO_2-TPD measurements and to Susana Domínguez for her administrative support.

Appendix A. Supporting information

Supplementary data associated with this article can be found in the online version at doi:10.1016/j.apcata.2025.120151.

Data availability

Data will be made available on request.

References

[1] M. Höök, X. Tang, Energy Policy 52 (2013) 797–809, https://doi.org/10.1016/j.enpol.2012.10.046.
[2] I. Capellán-Pérez, M. Mediavilla, C. de Castro, Ó. Carpintero, L.J. Miguel, Energy 77 (2014) 641–666, https://doi.org/10.1016/j.energy.2014.09.063.
[3] J.N. Chheda, G.W. Huber, J.A. Dumesic, Angew. Chem. Int. Ed. 46 (2007) 7164–7183, https://doi.org/10.1002/anie.200604274.
[4] J.J. Bozell, G.R. Petersen, Technology development for the production of biobased products from biorefinery carbohydrates—the US department of energy’s “Top 10” revisited, Green. Chem. 12 (2010) 539–554, https://doi.org/10.1039/b922014c.
[5] L.T. Mika, E. Cséfalvay, Á. Németh, Chem. Rev. 118 (2018) 505–613, https://doi.org/10.1021/acs.chemrev.7b00395.
[6] H.E., Hoydonckx, W.M. Van Rhijn, W. Van Rhijn, D.E. De Voss, P.A. Jacobs, in: Ullmann’s Encyclopedia of Industrial Chemistry, vol. 16, Wiley-VCH Verlag GmbH & Co. KGaA, Weinheim, 2012, pp. 285–313. https://doi.org/10.1002/14356007.a12_119.pub2.
[7] J.-P. Lange, Catal. Today 435 (2024) 114726, https://doi.org/10.1016/j.cattod.2024.114726.
[8] P. Khemthong, C. Yimsukanan, T. Narkkun, A. Srifa, T. Witoon, S. Pongchaiphol, S. Kiatphuengporn, K. Faungnawakij, Biomass. Bioenergy 148 (2021) 106033, https://doi.org/10.1016/j.biombioe.2021.106033.
[9] R. Mariscal, P. Maireles-Torres, M. Ojeda, I. Sádaba, M. López-Granados, Energy Environ. Sci. 9 (2016) 1144–1189, https://doi.org/10.1039/c5ee02666k.
[10] K. Gupta, R.K. Rai, S.K. Singh, ChemCatChem 10 (2018) 2326–2349, https://doi.org/10.1002/cctc.201701754.
[11] J. Zhu, G. Yin, ACS Catal. 11 (2021) 10058–10083, https://doi.org/10.1021/acscatal.1c01989.
[12] A. Jaswal, P.P. Singh, T. Mondal, Green. Chem. 24 (2022) 510–551, https://doi.org/10.1039/d1gc03278j.
[13] X. Zhang, S. Xu, Q. Li, G. Zhou, H. Xia, RSC Adv. 11 (2021) 27042–27058, https://doi.org/10.1039/d1ra04633k.
[14] N. Li, M.-H. Zong, ACS Catal. 12 (2022) 10080–10114, https://doi.org/10.1021/acscatal.2c02912.
[15] A. Bohre, S. Dutta, B. Saha, M.M. Abu-Omar, ACS Sustain. Chem. Eng. 3 (2015) 1263–1277, https://doi.org/10.1021/acssuschemeng.5b00271.
[16] C.-F. Chang, K. Paragian, S. Sadula, S. Rangarajan, D.G. Vlachos, ACS Sustain. Chem. Eng. 12 (2024) 12927–12937, https://doi.org/10.1021/acssuschemeng.4c04199.
[17] S. De, B. Saha, R. Luque, Bioresour. Technol. 178 (2015) 108–118, https://doi.org/10.1016/j.biortech.2014.09.065.
[18] M. Su, W. Li, Q. Ma, B. Zhu, J. Bioresour. Bioprod. 5 (2020) 256–265, https://doi.org/10.1016/j.jobab.2020.10.004.
[19] C.J. Barrett, J.N. Chheda, G.W. Huber, J.A. Dumesic, Appl. Catal. B 66 (2006) 111–118, https://doi.org/10.1016/j.apcatb.2006.03.001.

[20] M. Sauer, FEMS Microbiol Lett. 363 (2016) fnw134, https://doi.org/10.1093/femsle/fnw134.
[21] R.M. West, Z.Y. Liu, M. Peter, C.A. Gärtner, J.A. Dumesic, J. Mol. Catal. A Chem. 296 (2008) 18–27, https://doi.org/10.1016/j.molcata.2008.09.001.
[22] A. Bohre, M.I. Alam, K. Avasthi, F. Ruiz-Zepeda, B. Likozar, Appl. Catal. B 276 (2020) 119069, https://doi.org/10.1016/j.apcatb.2020.119069.
[23] A. Tampieri, M. Lilic, M. Constantí, F. Medina, Crystals 10 (2020) 833, https://doi.org/10.3390/cryst10090833.
[24] J. He, Q. Qiang, S. Liu, K. Song, X. Zhou, J. Guo, B. Zhang, C. Li, Fuel 306 (2021) 121765, https://doi.org/10.1016/j.fuel.2021.121765.
[25] X. Zhang, Y.Q. Li, C. Qian, L. An, W. Wang, X.F. Li, X.Z. Shao, Z. Li, RSC Adv. 13 (2023) 9466–9478, https://doi.org/10.1039/d3ra00906h.
[26] A. Tampieri, C. Russo, R. Marotta, M. Constantí, S. Contreras, F. Medina, 15 Appl. Catal. B 282 (2021) 119599, https://doi.org/10.1016/j.apcatb.2020.119599.
[27] G.J. Kelly, F. King, M. Kett, Green. Chem. 4 (2002) 392–399, https://doi.org/10.1039/b201982p.
[28] N.S. Biradar, A.M. Hengne, S.S. Sakate, R.K. Swami, C.V. Rode, Catal. Lett. 146 (2016) 1611–1619, https://doi.org/10.1007/s10562-016-1786-6.
[29] W. Shen, G.A. Tompsett, K.D. Hammond, R. Xing, F. Dogan, C.P. Grey, Appl. Catal. A Gen. 392 (2011) 57–68, https://doi.org/10.1016/j.apcata.2010.10.023.
[30] S. Rojas-Buzo, P. García-García, A. Corma, Green. Chem. 20 (2018) 3081–3091, https://doi.org/10.1039/c8gc00806j.
[31] D. Suttipat, W. Wannapakdee, T. Yutthalekha, S. Ittisanronnachai, T. Ungpittagul, K. Phomphrai, S. Bureekaew, C. Wattanakit, ACS Appl. Mater. Interfaces 10 (2018) 16358–16366, https://doi.org/10.1021/acsami.8b00389.
[32] S. Nishimura, A. Takagaki, K. Ebitani, Green. Chem. 15 (2013) 2026–2042, https://doi.org/10.1039/c3gc40405f.
[33] G.M. Lari, A.B.L. De Moura, L. Weimann, S. Mitchell, C. Mondelli, J. Pérez-Ramírez, J. Mater. Chem. A 5 (2017) 16200–16211, https://doi.org/10.1039/c7ta02061a.
[34] M. Mokhtar, A. Inayat, J. Ofili, W. Schwieger, Appl. Clay Sci. 50 (2010) 176–181, https://doi.org/10.1016/j.clay.2010.07.019.
[35] K. Kaneda, T. Mizugaki, Green. Chem. 21 (2019) 1361–1389, https://doi.org/10.1039/c8gc03391a.
[36] S. Abelló, D. Vijaya-Shankar, J. Pérez-Ramírez, Appl. Catal. A Gen. 342 (2008) 119–125, https://doi.org/10.1016/j.apcata.2008.03.010.
[37] M.G. Álvarez, D. Tichit, F. Medina, J. Llorca, Appl. Surf. Sci. 396 (2017) 821–831, https://doi.org/10.1016/j.apsusc.2016.11.037.
[38] S. Abelló, F. Medina, D. Tichit, J. Pérez-Ramírez, X. Rodríguez, J.E. Sueiras, P. Salagre, Y. Cesteros, Appl. Catal. A Gen. 281 (2005) 191–198, https://doi.org/10.1016/j.apcata.2004.11.037.
[39] O. Kikhtyanin, Z. Tišler, R. Velvarská, D. Kubička, Appl. Catal. A Gen. 536 (2017) 85–96, https://doi.org/10.1016/j.apcata.2017.02.020.
[40] S. Abelló, F. Medina, D. Tichit, J. Pérez-Ramírez, J.C. Groen, J.E. Sueiras, P. Salagre, Y. Cesteros, Chem. Eur. J. 11 (2005) 728–739, https://doi.org/10.1002/chem.200400409.
[41] P. Scherrer, Nachr. Ges. Wiss. Goettingen, Math. Phys. Kl. 1918 (1918) 98–100.
[42] H. Chang, A.H. Motagamwala, G.W. Huber, J.A. Dumesic, Green. Chem. 21 (2019) 5532–5540, https://doi.org/10.1039/c9gc01859j.
[43] M. Thommes, K. Kaneko, A.V. Neimark, J.P. Olivier, F. Rodriguez-Reinoso, J. Rouquerol, K.S.W. Sing, Pure Appl. Chem. 87 (2015) 1051–1069, https://doi.org/10.1515/pac-2014-1117.
[44] J.T. Kloprogge, L. Hickey, R.L. Frost, J. Raman Spectrosc. 35 (2004) 967–974, https://doi.org/10.1002/jrs.1244.
[45] S. Abelló, F. Medina, D. Tichit, J. Pérez-Ramírez, J.E. Sueiras, P. Salagre, Y. Cesteros, Appl. Catal. B. 70 (2007) 1–4, https://doi.org/10.1016/j.apcatb.2006.01.021.
[46] C. Xu, Y. Gao, X. Liu, R. Xin, Z. Wang, RSC Adv. 3 (2013) 793–801, https://doi.org/10.1039/c2ra21762g.
[47] K. Nakamoto, Infrared and Raman spectra of inorganic and coordination compounds, John Wiley & Sons, Hoboken, 1997.
[48] J. Horáček, Z. Tišler, U. Akhmetzyanova, P.G. Chirila, H. de Paz Carmona, Reac. Kinet. Mech. Cat. 133 (2021) 341–353, https://doi.org/10.1007/s11144-021-01976-z.
[49] A. Tampieri, K. Föttinger, N. Barrabés, F. Medina, Appl. Catal. B Environ. 319 (2022) 121889, https://doi.org/10.1016/j.apcatb.2022.121889.
[50] T. Hibino, A. Tsunashima, Chem. Mater. 10 (1998) 4055–4061, https://doi.org/10.1021/cm980478q.
[51] V. Korolova, O. Kikhtyanin, F. Ruiz-Zepeda, M. Lhotka, M. Veselý, D. Kubička, Appl. Catal. A Gen. 632 (2022) 118482, https://doi.org/10.1016/j.apcata.2022.118482.